npj | Quantum Materials

www.nature.com/npjquantmats

ARTICLE OPEN

Check for updates

Quest for quantum states via field-altering technology

Gang Cao[1]✉, Hengdi Zhao[1], Bing Hu[1,2], Nicholas Pellatz[1], Dmitry Reznik[1], Pedro Schlottmann[3] and Itamar Kimchi[1]

We report quantum phenomena in spin-orbit-coupled single crystals that are synthesized using an innovative technology that "field-alters" crystal structures via application of magnetic field during crystal growth. This study addresses a major challenge facing the research community today: A great deal of theoretical work predicting exotic states for strongly spin-orbit-coupled, correlated materials has thus far met very limited experimental confirmation. These conspicuous discrepancies are due in part to the extreme sensitivity of these materials to structural distortions. The results presented here demonstrate that the field-altered materials not only are much less distorted but also exhibit phenomena absent in their non-altered counterparts. The field-altered materials include an array of *4d* and *5d* transition metal oxides, and three representative materials presented here are $Ba_4Ir_3O_{10}$, Ca_2RuO_4, and Sr_2IrO_4. This study provides an approach for discovery of quantum states and materials otherwise unavailable.

npj Quantum Materials (2020)5:83 ; https://doi.org/10.1038/s41535-020-00286-2

INTRODUCTION

The discovery of quantum states requires innovative approaches. Here, we report quantum phenomena in single crystals of *4d*- and *5d*-electron based oxides obtained through structurally altering materials via application of magnetic field during materials growth–A magnetic field aligns magnetic moments and, through strong spin-orbit interactions (SOI) and magnetoelastic coupling, alters crystal structures at high temperatures, as schematically illustrated in Fig. 1a. This work demonstrates that such a field-altering technology is highly effective for quantum materials with a delicate interplay between SOI and comparable Coulomb correlations, in which exotic quantum states may arise whenever competing interactions conspire to provoke unusually large susceptibilities to small stimuli[1–7].

The field-altering technology addresses a major challenge to today's research community: a great deal of theoretical work that predicts exotic states for correlated and spin-orbit-coupled oxides has thus far met limited experimental confirmation[1,2,6–15]. We have long recognized that the conspicuous discrepancies between current theory and experiment are due in part to the extreme susceptibility of relevant materials to structural distortions and disorder[2,3]. The field-altering technology addresses this challenge by field-altering materials via application of magnetic field during materials growth (Fig. 1a), and this study demonstrates that it works particularly well for materials whose low energy physics is dictated by competing interactions[1–3,6–15] leading to multiple nearly degenerate states. Consequently, a resulting alteration in structural distortions (e.g., rotations/tilt of octahedra or Ir-O-Ir, and Ru-O-Ru bond angles) can be associated with disproportionately strong responses in physical properties, facilitating a different ground state to emerge[2,6,16–24]. We would like to emphasize a crucial role of the bond angles that can significantly affect the physical properties via strong SOI and magnetoelastic coupling[2,6,17,18,20,22,24,25]. The field-altering technology allows the Zeeman effect to exert a torque on the spin, which couples to the orbit via SOI; the orbit in turn needs to readjust and tilts the octahedron, thus altering the bond angles. The hopping matrix elements of the *d*-electrons depends strongly on the rotating/tilting angle, and so does the superexchange via the Kanamori rules. Hence, small changes in the bond angles cause disproportionately large electronic changes, emphasizing the critical role that SOI plays in this class of materials in which the electronic and ionic sectors are strongly coupled.

We show that such drastic changes in physical properties are a consequence of field-altering with a very weak magnetic field no stronger than 0.06 Tesla (see for instance Fig. 1b-c). This is utterly inconsistent with conventional thermodynamics, according to which even an extremely strong magnetic field (e.g., 45 Tesla ~ 4 meV) would seem inconsequential to chemical reactions as magnetic contributions to the Gibbs free enthalpy are too small to be significant in terms of energy scale[26]. Indeed, previous literature on applying magnetic fields during crystal growth of silicon[27–29] and protein crystals[30] were limited to only change striation of the crystals, i.e., surface patterns of the grown crystals[27]. No reports show synthesis effects of applied magnetic field on structural and physical properties. This work puts forward an approach for an otherwise unavailable path to discovery of quantum states/materials.

Here, we report results of our study on three representative single-crystal materials that are field-altered and our controlled study on their non-altered counterparts. These three materials are $Ba_4Ir_3O_{10}$[31], Sr_2IrO_4[32], and Ca_2RuO_4[33]. This comprehensive investigation involves an array of *4d* and *5d* oxides. The study of all these materials reveals a common empirical trend that the field-altered materials are much less distorted than their non-altered counterparts, and exhibit quantum states that are either absent or vastly different from those in the non-altered materials.

Experimental details are presented in the Supplemental Information (SI) (Supplemental Information, experimental and theoretical details). A few crucial details are worth mentioning here. The field-altered crystals are grown in a 1500 °C-furnace carefully surrounded with two specially-made permanent magnets, each of which is of 1.4 Tesla (Fig. 1a). Since the magnetic field of a permanent magnet decays with distance *d* as $1/d^3$, the actual strength of the magnetic field inside the furnace chamber is measured to be within a range of 0.02–0.06 Tesla. The non-altered single crystals are synthesized without the applied magnetic field in otherwise identical conditions. All results are repeatedly confirmed by samples from multiple batches of single crystals

[1]Department of Physics, University of Colorado at Boulder, Boulder, CO 80309, USA. [2]School of Mathematics and Physics, North China Electric Power University, 102206 Beijing, China. [3]Department of Physics, Florida State University, Tallahassee, FL 32306, USA. ✉email: gang.cao@colorado.edu

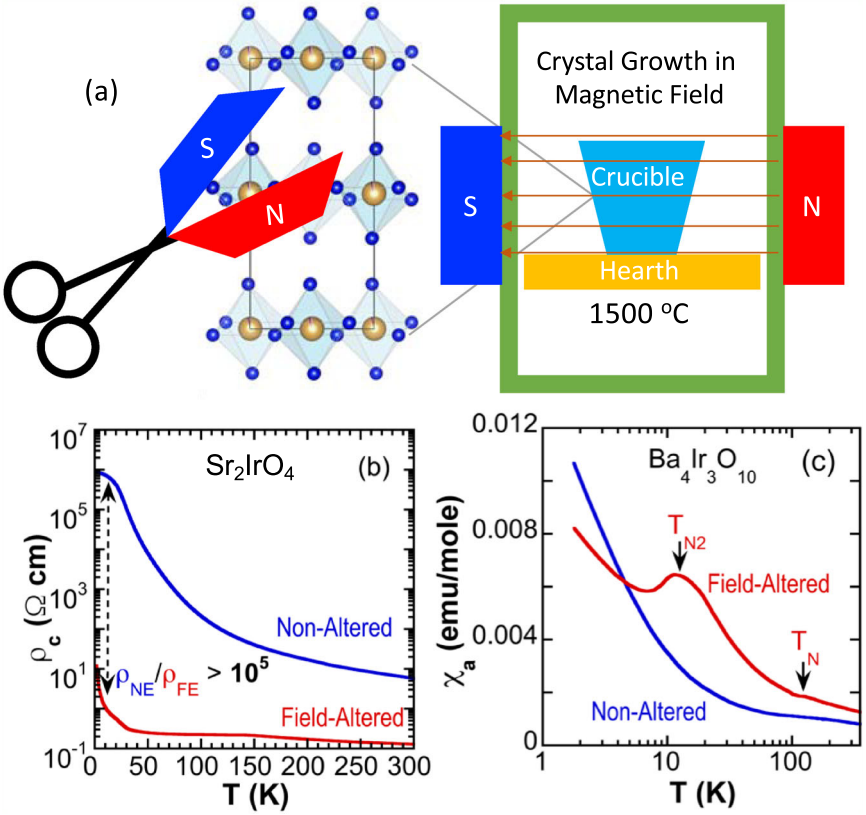

Fig. 1 Field-altering technology. (**a**) A schematic for field-altering a crystal structure (left) during crystal growth in the molten-zone sandwiched between the two magnets (right). Contrasting physical properties of two exemplary materials to highlight field-altering effects: (**b**) Sr_2IrO_4: the *c*-axis resistivity ρ_c is five orders of magnitude smaller in the field-altered crystal (red) than in the non-altered counterpart (blue); (**c**) $Ba_4Ir_3O_{10}$: a comparison of the *a*-axis magnetic susceptibility χ_a between the non-altered crystal (blue) that features a quantum liquid and the field-altered crystal (red) that becomes an antiferromagnet with two magnetic transitions.

synthesized throughout the nearly one-year period of this study. The field-altered single crystals are of high-quality and purity. See Supplementary Figs. 1, 2, 3, 4, 5, and 6 for Bragg peaks and rocking curves for both the field-altered and non-altered single crystals in SI. These data further demonstrate the high quality of these crystals. In particular, the X-ray diffraction data in SI illustrate sharp, nearly delta-function Bragg peaks in the field-altered crystals. This is not surprising in part because of field altering. Recall effects such as thermal fluctuations merely reduce Bragg peak magnitudes by a Debye-Waller factor but preserve their delta-function sharpness, as indicated in Supplementary Figs. 1–6. The modified synthesis conditions due to field altering change the equilibrium point (i.e., the bond angle and hence the physical properties) or create a new minimum and hence a different phase, as compared to the synthesis conditions without magnetic field.

The work presented here can serve as proof-of-concept results; the field-altering technology with much stronger magnetic fields will result in more discoveries of quantum states and materials.

RESULTS AND DISCUSSION

$Ba_4Ir_3O_{10}$: from quantum liquid to correlated magnet

The magnetic insulator $Ba_4Ir_3O_{10}$ was recently found to be a quantum liquid[34]. As shown in Fig. 2, $Ba_4Ir_3O_{10}$ is structurally a two-dimensional, square lattice with no apparent spin chains. Our recent study reveals a quantum liquid persisting down to 0.2 K with Curie-Weiss temperature, θ_{CW}, ranging from −766 K to −169 K due to magnetic anisotropy. The anisotropy-averaged frustration parameter, defined as $f = |\theta_{CW}|/T_N$, is more than 2000, seldom seen in other materials. Heat capacity and thermal conductivity are both linear at low temperatures, a defining characteristic for an exotic quantum liquid state. The novelty of the state is that frustration occurs in an apparently un-frustrated square lattice which features Ir_3O_{12} trimers of face-sharing IrO_6 octahedra. It is these trimers that play a crucial role in frustration. In particular, a combined effect of the direct (Ir-Ir) and superexchange (Ir-O-Ir) interactions in the trimers results in such a delicate coupling that the middle Ir ion in a trimer is relatively weakly linked to the two neighboring Ir ions. Pure inter-trimer couplings generate an effective one-dimensional system with zigzag chains or Luttinger liquids along the *c* axis; restoring the relatively weak but crucial intra-trimer couplings can preserve a 1D or 2D quantum liquid[34].

This intricacy is fundamentally changed in the field-altered $Ba_4Ir_3O_{10}$. Structurally, the field-altered single crystal exhibits a significant elongation in the *b* axis with only slight changes in the *a* and *c* axis. As a result, the unit cell volume *V* increases considerably by up to 0.54% at 350 K (see Fig. 2a-c). Remarkably, both the Ir-Ir bond distance within each trimer and the Ir-O-Ir bond angle between trimers increase sizably (Fig. 2f-g).

The effect of field-altering readily destroys the quantum liquid and stabilizes a robust, long-range magnetic order. As shown in Fig. 3a, two magnetic anomalies occur at Néel temperatures $T_N = 125$ K and $T_{N2} = 12$ K in the field-altered sample (solid dots), sharply contrasting the magnetic behavior of the non-altered sample (dashed lines). Consequently, the absolute values of the Curie-Weiss temperature θ_{CW} are considerably reduced and become comparable to $T_N = 125$ K for the field-altered sample (Fig. 3b-c); the corresponding frustration parameter f ($=|\theta_{CW}|/T_N$) is drastically reduced to a value less than 3 from 2000 for the

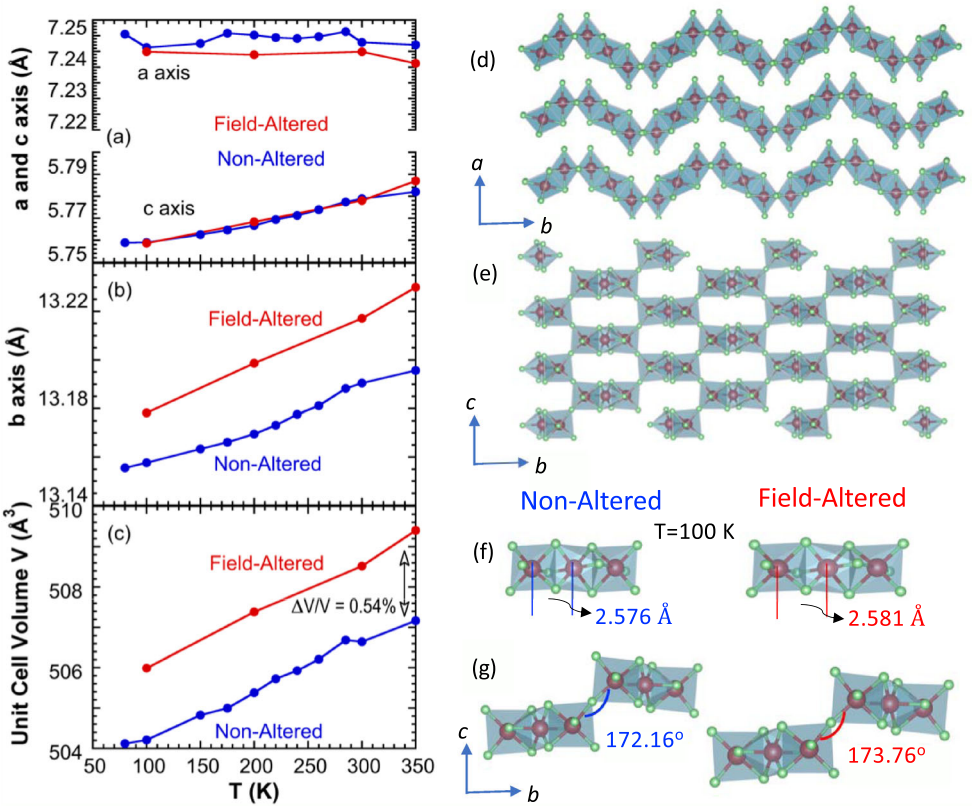

Fig. 2 $Ba_4Ir_3O_{10}$: structural properties of the field-altered (in red) and non-altered (in blue) single crystals. The temperature dependence of the lattice parameters (**a**) the *a* and *c* axis, (**b**) the *b* axis and (**c**) the unit cell volume *V*. (**d**) and (**e**) the crystal structure in the *ab* and *bc* plane, respectively. (**f**) The Ir-Ir bond distance within a trimer. (**g**) The Ir-O-Ir bond angle between corner-sharing trimers (the marked values are for 100K).

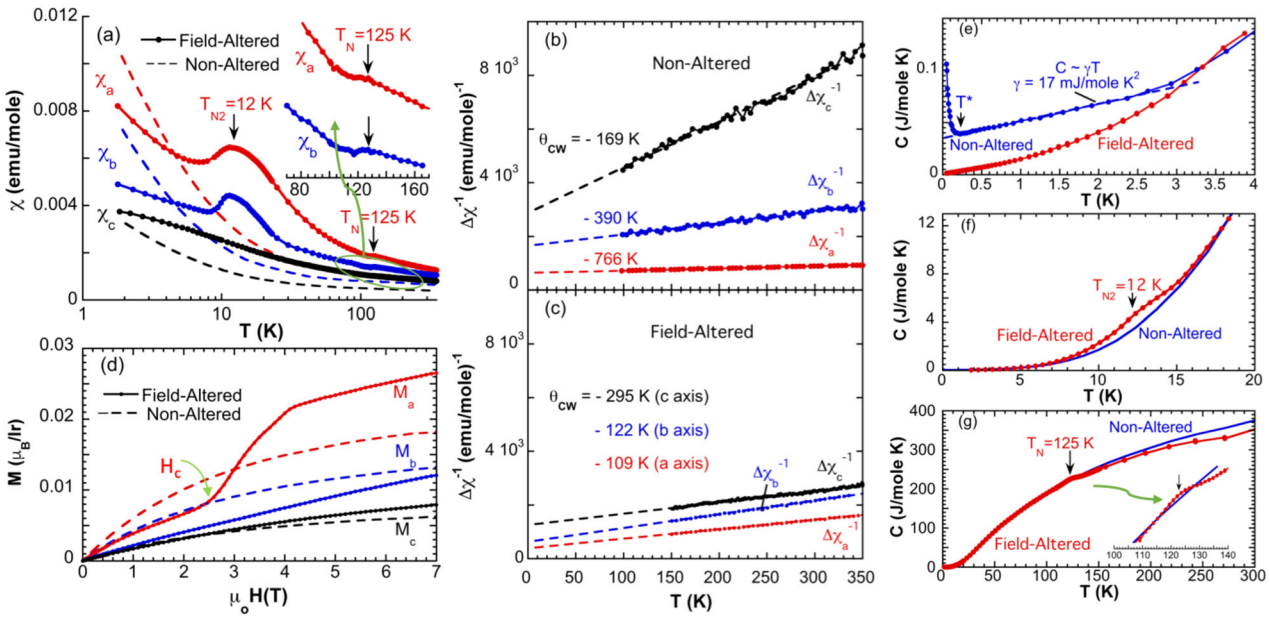

Fig. 3 $Ba_4Ir_3O_{10}$: physical properties of the field-altered and non-altered single crystals. The temperature dependence for the *a*, *b* and *c* axis of (**a**) the magnetic susceptibility $\chi(T)$ for the field-altered (solid dots) (Inset: zoomed-in χ near T_N), and the non-altered (dashed lines) samples, and $\Delta\chi^{-1}$ (**b**) for the non-altered single crystal and (**c**) for the field-altered single crystal. (**d**) The isothermal magnetization M(H) at 1.8K for the field-altered (solid lines) and the non-altered (dashed lines) samples. The temperature dependence of the heat capacity C(*T*) for the field-altered (red) and the non-altered (blue) samples at (**e**) the lowest temperatures, (**f**) the intermediate temperatures and (**g**) the high temperatures. The inset in (**g**): the zoomed-in C(*T*) near T_N.

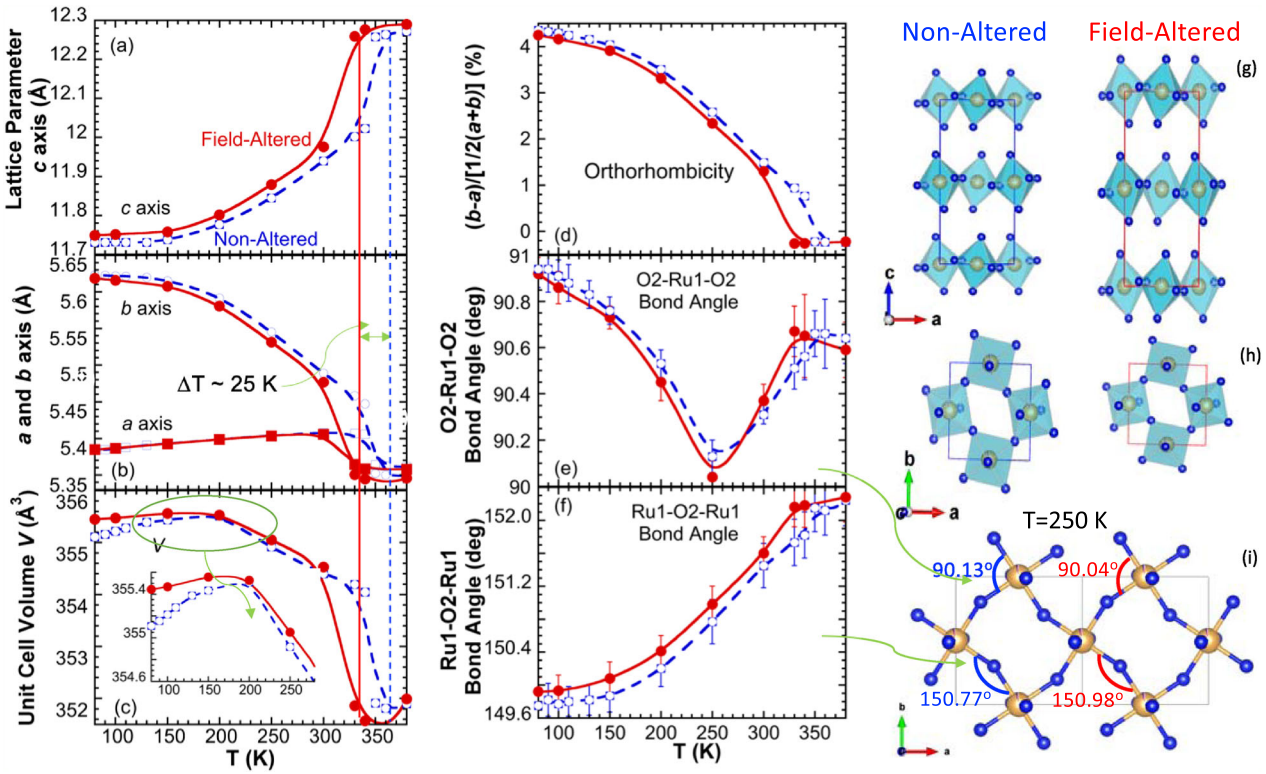

Fig. 4 Ca_2RuO_4: structural properties of the field-altered (in red) and non-altered (in blue) single crystals. The temperature dependence of the lattice parameters (**a**) the *c* axis, (**b**) the *a* and *b* axis, (**c**) the unit cell volume *V*, (**d**) the basal plane orthorhombicity, (**e**) the O2-Ru1-O2 bond angle and (**f**) the Ru1-O2-Ru1bond angle. Note that the error bars are defined as standard deviation (s.d.). (**g**) and (**h**) The crystal structure in the ac and ab plane, respectively. (**i**) The schematic for the O2-Ru1-O2 and Ru1-O2-Ru1bond angles for the field-altered (red) and non-altered (blue) structures at 250 K.

non-altered sample[34], indicating a complete removal of frustration. The long-range magnetic order is corroborated by a metamagnetic transition at a critical field $\mu_o H_c = 2.5$ T along the *a* axis, as shown in Fig. 3d.

The heat capacity, which measures bulk effects, confirms the antiferromagnetic (AFM) order. In particular, the low-temperature linearity of the heat capacity C(*T*) (data in blue Fig. 3e), which characterizes the gapless excitations in the non-altered sample, is replaced by the T^3-dependence in the field-altered sample, which is anticipated for an insulating antiferromagnet (data in red in Fig. 3e). The sharp upturn in C(*T*) at $T^* = 0.2$ K in the non-altered sample also disappears in the field-altered sample. As temperature rises, two anomalies occur at $T_{N2} = 12$ K (Fig. 3f) and $T_N = 125$ K (Fig. 3g), respectively, confirming the robustness of the long-range magnetic order. In short, the quantum liquid in the non-altered $Ba_4Ir_3O_{10}$[34] is replaced by the AFM state in the field-altered $Ba_4Ir_3O_{10}$.

Ca_2RuO_4: from antiferromagnet to weak ferromagnet

The AFM insulator Ca_2RuO_4 exhibits a metal-insulator transition at $T_{MI} = 357$ K[33,35], which marks a concomitant, violent structural transition with a severe rotation and tilt of RuO_6. This structural transition removes the t_{2g} orbital degeneracy (d_{xy}, d_{yz}, d_{zx}), which dictates the physical properties of Ca_2RuO_4[22,36–46]. An AFM transition occurs only at a considerably lower Neel temperature $T_N = 110$ K[33], highlighting its close association with a further distorted structure.

As shown in Fig. 4, the crystal structure of Ca_2RuO_4 is significantly field-altered, becoming less distorted. A few changes are particularly remarkable. The first-order structural transition T_{MI} is suppressed by about 25 K from 357 K to 332 K, which is marked by the vertical blue dashed and red solid lines, respectively, through Fig. 4a–c. In the field-altered structure, the *c* axis gets longer (Fig. 4a); the *b* axis becomes shorter whereas the *a* axis changes very slightly (Fig. 4b), thus leading to a reduced orthorhombicity (Fig. 4d). More importantly, the O2-Ru1-O2 and Ru1-O2-Ru1 bond angles, which measure the octahedral rotation and tilt, get relaxed, in the field-altered structure (Fig. 4e-f). These lattice changes are critical to both transport and magnetic properties. The crystal structure in the *ac* and *ab* planes and the schematic for the bond angles are shown in Fig. 4g-i. Remarkably, the structural alterations are more significant at high temperatures than at low temperatures. However, changes in the physical properties are drastic at low temperatures, as seen below, suggesting high sensitivity of the electronic structure to even slight changes in the lattice, particularly, the bond angles.

Indeed, the *a*-axis electrical resistivity ρ_a of the field-altered sample shows a much lower metal-insulator transition T_{MI} at 324 K, 31 K lower than T_{MI} for the non-altered sample, as seen in Fig. 5a. The suppressed T_{MI} closely tracks the structural transition that is reduced by about 25 K in the field-altered sample (Fig. 4).

Magnetically, the field-altered sample behaves vastly differently from the non-altered sample. In particular, the *a*-axis magnetization M_a of the field-altered sample shows a ferromagnetic-like behavior with a distinct temperature dependence below T_N (red curves), in sharp contrast to that of the non-altered sample (blue curve) (see Fig. 5b). Moreover, a large hysteresis behavior of M_a is also observed in the field-altered sample, which is expected in a ferromagnet or weak ferromagnet, as illustrated in Fig. 5c. This behavior is in sharp contrast to that of the non-altered Ca_2RuO_4[3,30]. The magnetic changes are also in accordance with changes in the low-temperature heat capacity C(*T*). For an

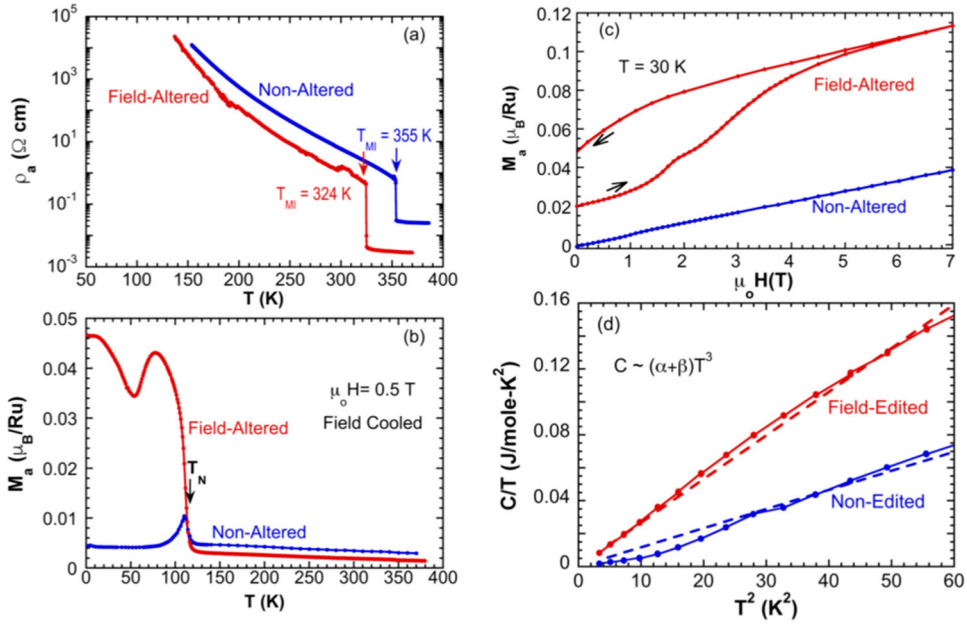

Fig. 5 Ca_2RuO_4: physical properties of the field-altered (in red) and non-altered (in blue) single crystals. The temperature dependence of (**a**) the *a*-axis electrical resistivity ρ_a and (**b**) the *a*-axis magnetic susceptibility $M_a(T)$ at $\mu_oH = 0.5T$. **c** The *a*-axis isothermal magnetization $M_a(H)$ at 30 K. (**d**) The low-temperature heat capacity C(*T*) plotted as *C*/*T* vs T^2.

insulating antiferromagnet, $C(T) \sim (\alpha + \beta)\, T^3$, in which the first term α and the second term β are associated with magnon and phonon contributions to C(*T*), respectively. Here, C(*T*) shows a significant slope change defined by $(\alpha + \beta)$ in the plot of *C*/*T* vs T^2 in Fig. 5d. Such a slope change clearly points out that the emergent magnetic state is distinctly different from the native AFM state, consistent with the magnetic data in Fig. 5b-c.

Sr_2IrO_4: towards metallic state

Sr_2IrO_4 is an archetype of the spin-orbit-coupled magnetic insulator[47,48]. It is widely anticipated that with slight electron doping, Sr_2IrO_4 should be a novel superconductor[2,9–12,24]. However, there has been no experimental confirmation of superconductivity, despite many years of experimental effort[2]. We believe that the absence of the predicted superconductivity is due to inherently severe structural distortions that suppress superconductivity[2,16–18,49]. A theoretical study similarly attributes the lack of superconductivity to the octahedral rotation[24]. Indeed, a recent neutron study reveals an anomalous change in the Ir-O-Ir bond angle below 50 K, which directly links to the anomalous transport and magnetic properties in Sr_2IrO_4[25]. In fact, it is precisely because of this early realization that we initiated the development of the field-altering technology and investigations of field-altered materials. Certainly, the structural and physical properties of the field-altered Sr_2IrO_4 and 3% La doped Sr_2IrO_4 are drastically improved, compared to those of the non-altered samples. In particular, the field-altered structure is less distorted with a greater Ir-O-Ir bond angle (Fig. 6a-b), and the AFM transition T_N is suppressed by astonishing 90 K (Fig. 6c); the isothermal magnetization is reduced by 50% and much less "saturated" compared to that for the non-altered Sr_2IrO_4 (see Supplementary Fig. 7). That the Ir-O-Ir bond angle dictates T_N and M suggests a critical role of the Dzyaloshinskii-Moriya interaction[6]. Such magnetic changes are clearly reflected in Raman scattering. One-magnon Raman scattering measures the anisotropy field that pins the magnetic moment orientation. It broadens with increasing temperature and vanishes at T_N. At 10 K, this peak in the non-altered Sr_2IrO_4 occurs near 18 cm^{-1} (data in blue in Fig. 6d)[50] but is absent in the field-altered Sr_2IrO_4 for the measured energy range (data in red Fig. 6d). This conspicuous disappearance of the peak indicates that the anisotropy field is drastically reduced and, consequently, the one-magnon peak is either completely removed or suppressed to an energy below the energy cutoff of 5.3 cm^{-1} (0.67 meV) in the field-altered sample. On the other hand, two-magnon scattering remains essentially unchanged (see Supplementary Fig. 8). Note the broadened peak in the field-altered sample in Fig. 6c is a result of the weakened AFM state.

Furthermore, the electrical resistivity for both the *a* and *c* axis, ρ_a and ρ_c, is reduced by up to five orders of magnitude and shows a nearly metallic behavior at high temperatures in the field-altered Sr_2IrO_4 (Fig. 6e-f)! This is consistent with the effect of the relaxed Ir-O-Ir bond angle, which enhances electron hopping. Note that the hugely reduced resistivity also rules out any potential crystalline imperfectness caused by field altering. An anomaly corresponding to $T_N = 150$ K (Inset in Fig. 6e) indicates a close correlation between the transport and magnetic properties that is noticeably absent in the non-altered Sr_2IrO_4[2]. The resistivity for the field-altered $(Sr_{0.97}La_{0.03})_2IrO_4$ exhibits an abrupt drop below 20 K by nearly three orders of magnitude, suggesting that the long-elusive superconductivity in the iridate may be finally within reach (these results to be reported in a separate paper).

Proposed proof-of-concept theoretical mechanism

The tiny fields of 200 gauss sufficient for field-altering involve a magnetic Zeeman energy scale of only 0.002 meV per spin-1/2, orders of magnitude smaller than typical electronic energy scales. While high temperature magnetohydrodynamic effects are expected to also play a role here similar to the role they play in other systems, an additional, qualitatively new mechanism is necessary to explain the present observations: What energetic mechanism could allow the weak magnetic field to alter the crystal structure so drastically as to change local bond angles by even a few percent, which accompanies the enormous changes in the physical properties discussed above?

Here we suggest a proof of concept of such a qualitatively new mechanism for field altering, based on a combined effect of (1)

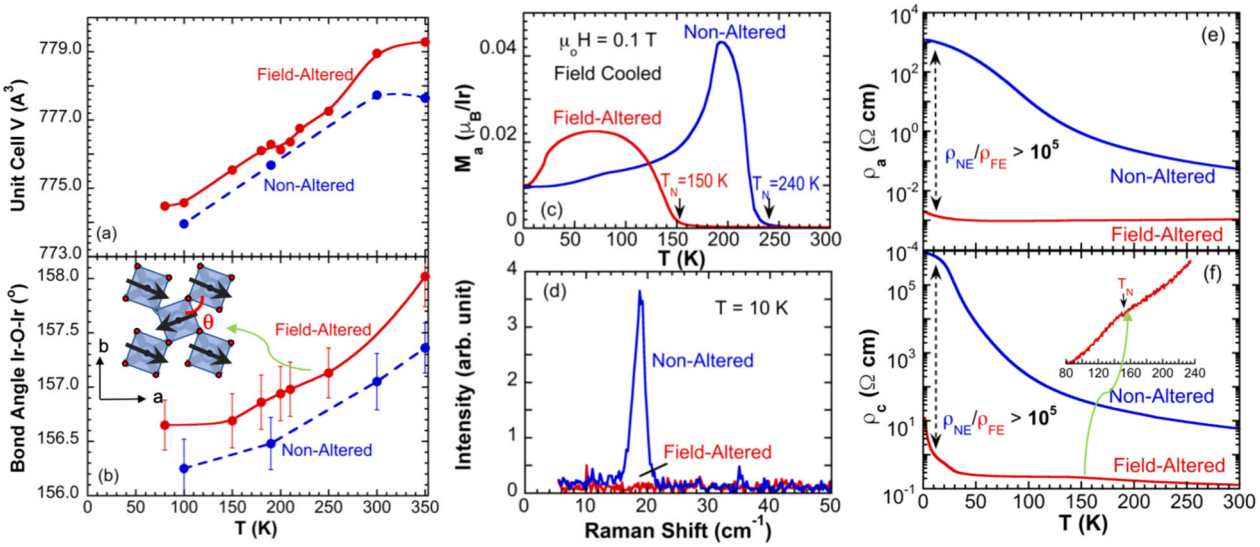

Fig. 6 Sr_2IrO_4: structural and physical properties of the field-altered (in red) and non-altered (in blue) single crystals. The temperature dependence of (**a**) the unit cell volume *V*, (**b**) the Ir-O-Ir bond angle θ (Inset illustrates θ) and (**c**) the *a*-axis magnetization M_a at $\mu_oH = 0.1T$. Note that the error bars are defined as standard deviation (s.d.). (**d**) The Raman single-magnon peak at 10K. The temperature dependence of (**e**) the *a*-axis resistivity ρ_a and (**f**) the *c*-axis resistivity ρ_c for Sr_2IrO_4. Note that both ρ_a and ρ_c drop by up to five orders of magnitude. Inset: the anomaly in ρ_a at T_N for the field-altered crystal.

strong SOI or magnetoelastic coupling, and (2) magnetic frustration. See the SI for technical details. As an example, consider the square lattice quantum compass model[51], a term argued to arise in the effective description of Sr_2IrO_4[6] and, by symmetry considerations, of Ca_2RuO_4. For this model, the degeneracy of the manifold containing each state, and the divergent negative free energy for defect states, implies that even infinitesimally small magnetic fields have a singular and large effect on the free energy landscape. The spin-orbit and magnetoelastic couplings imply that each defect in the effective-spin texture also produces a change in the local orbitals and local distortions of the crystal. When the full Hamiltonian still results in magnetic frustration, as indeed is observed in all three non-altered compounds discussed above, the frustrated system no longer has degenerate manifolds but instead shows a glass-like landscape of states, some of which lie nearby in energy but have drastically different spin configurations. During synthesis of materials with this free energy landscape, even a small magnetic field can have a large effect on the dynamics of the crystal distortion relaxation and electronic structure. See Supplementary Discussion and Supplementary References. The propose mechanism could serve as a starting point for eventually reaching a full understanding of field altering at high temperatures.

In short, all experimental results presented above demonstrate that the field-altering technology is extraordinarily effective for modifying quantum states in correlated and spin-orbit-coupled materials. With stronger magnetic fields, this technology should overcome more materials challenges, leading to more discoveries of quantum states and materials that cannot be produced otherwise.

METHODS

Single crystal synthesis and characterization

Single crystals of $Ba_4Ir_3O_{10}$, Ca_2RuO_4 and Sr_2IrO_4 were grown using a flux method. The mixtures were fired at 1460 C, 1420 C, and 1470 C for $Ba_4Ir_3O_{10}$, Ca_2RuO_4, and Sr_2IrO_4, respectively, for 10–15 h and then slowly cooled to room temperature at a rate of 4 C/h. Platinum crucibles were used. The average sample size for $Ba_4Ir_3O_{10}$ is ~$3 \times 2 \times 1$ mm^3 and smaller for Ca_2RuO_4 and Sr_2IrO_4. Measurements of crystal structures were performed using a Bruker Quest ECO single-crystal diffractometer equipped with a PHOTON 50 CMOS detector. It is also equipped with an Oxford Cryosystem that creates sample temperature environments ranging from 80 K to 400 K during x-ray diffraction measurements. Chemical analyses of the samples were performed using a combination of a Hitachi MT3030 Plus Scanning Electron Microscope and an Oxford Energy Dispersive X-Ray Spectroscopy. Magnetic properties were measured using a Quantum Design (QD) MPMS-7 SQUID Magnetometer with a rotator that enables angular measurements of magnetic properties. Standard four-lead measurements of the electrical resistivity were carried out using a QD Dynacool PPMS System equipped with a 14-Tesla magnet. The heat capacity was measured down to 0.05 K using a dilution refrigerator for the PPMS.

Two permanent magnets, each of which is of 1.4 Tesla and "8" in diameter, are aligned and mounted on the two opposite sides of a 1500 C box furnace (see Fig. 1 in main text). The resultant strength of the applied magnetic field inside the furnace chamber varies from 0.02 to 0.06 Tesla, sensitively depending on the location.

Raman scattering measurements

Raman scattering measurements were performed using a 671 nm diode-pumped solid-state laser in a back-scattering geometry. Scattered light was collected and focused onto the entrance slit of a custom McPherson triple stage spectrometer equipped with a liquid-nitrogen-cooled CCD detector. Field-altered and non-altered samples of Sr_2IrO_4 were cleaved in air to achieve a mirror-like surface before being loaded into a closed-cycle refrigerator.

DATA AVAILABILITY

The data that support the findings of this study are available from the corresponding author upon reasonable request.

Received: 10 August 2020; Accepted: 15 October 2020;
Published online: 09 November 2020

REFERENCES

1. Witczak-Krempa, W., Chen, G., Kim, Y. B. & Balents, L. Correlated quantum phenomena in the strong spin-orbit regime. *Annu. Rev. Condens. Matter Phys.* **5**, 57–82 (2014).

2. Cao, G. & Schlottmann, P. The challenge of spin–orbit-tuned ground states in iridates: a key issues review. *Rep. Prog. Phys.* **81**, 042502 (2018).
3. Cao, G. & DeLong, L., Frontiers of 4d- and 5d-transition metal oxides Ch 6 and Ch 8 (World Scientific, Singapore, 2013).
4. Tokura, Y., Kawasaki, M. & Nagaosa, N. Emergent functions of quantum materials. *Nat. Phys.* **13**, 1056–1068 (2017).
5. Basov, D. N., Averitt, R. D. & Hsieh, D. Towards properties on demand in quantum materials. *Nat. Mater.* **16**, 1077–1088 (2017).
6. Jackeli, G. & Khaliullin, G. Mott insulators in the strong spin-orbit coupling limit: from Heisenberg to a quantum compass and Kitaev models. *Phys. Rev. Lett.* **102**, 017205 (2009).
7. Pesin, D. & Balents, L. Mott physics and band topology in materials with strong spin–orbit interaction. *Nat. Phys.* **6**, 376–381 (2010).
8. Wan, X. G., Turner, A. M., Vishwanath, A. & Savrasov, S. Y. Topological semimetal and Fermi-arc surface states in the electronic structure of pyrochlore iridates. *Phys. Rev. B* **83**, 205101 (2011).
9. Wang, F. & Senthil, T. Twisted Hubbard Model for Sr_2IrO_4: magnetism and possible high temperature superconductivity. *Phys. Rev. Lett.* **106**, 136402 (2011).
10. Watanabe, H., Shirakawa, T. & Yunoki, S. Monte Carlo study of an unconventional superconducting phase in iridium oxide $J_{eff} = 1/2$ Mott insulators induced by carrier doping. *Phys. Rev. Lett.* **110**, 027002 (2013).
11. Meng, Z. Y., Kim, Y. B. & Kee, H. Y. Odd-parity triplet superconducting phase in multiorbital materials with a strong spin-orbit coupling: Application to doped Sr_2IrO_4. *Phys. Rev. Lett.* **113**, 177003 (2014).
12. Yang, Y. et al. Superconductivity in doped Sr_2IrO_4: a functional renormalization group study. *Phys. Rev. B* **89**, 094518 (2014).
13. You, Y. Z., Kimchi, I. & Vishwanath, A. Doping a spin-orbit Mott insulator: topological superconductivity from the Kitaev-Heisenberg model and possible application to $(Na_2/Li_2)IrO_3$. *Phys. Rev. B* **86**, 085145 (2012).
14. Chaloupka, J., Jackeli, G. & Khaliullin, G. Kitaev-Heisenberg model on a honeycomb lattice: Possible exotic phases in iridium oxides A_2IrO_3. *Phys. Rev. Lett.* **105**, 027204 (2010).
15. Rau, J. G., Lee, E. K. H. & Kee, H. Y. Spin-orbit physics giving rise to novel phases in correlated systems: Iridates and related materials. *Annu. Rev. Condens. Matter Phys.* **7**, 195–221 (2016).
16. Chikara, S. et al. Giant magnetoelectric effect in the $J_{eff} = 1/2$ Mott insulator Sr_2IrO_4. *Phys. Rev. B* **80**, 140407(R) (2009).
17. Korneta, O. B. et al. Electron-doped $Sr_2IrO_{4-\delta}$ ($0 \le \delta \le 0.04$): evolution of a disordered $J_{eff} = 1/2$ Mott insulator into an exotic metallic state. *Phys. Rev. B* **82**, 115117 (2010).
18. Ge, M. et al. Lattice-driven magnetoresistivity and metal-insulator transition in single-layered iridates. *Phys. Rev. B* **84**, 100402(R) (2011).
19. Wang, J. C. et al. Lattice-tuned magnetism of $Ru^{4+}(4d^4)$ ions in single-crystals of the layered honeycomb ruthenates: Li_2RuO_3 and Na_2RuO_3. *Phys. Rev. B.* **90**, 161110 (R) (2014).
20. Cao, G. et al. Electrical control of structural and physical properties via spin-orbit interactions in Sr_2IrO_4. *Phys. Rev. Lett.* **120**, 017201 (2018).
21. Zheng, H. et al. Observation of a pressure-induced transition from interlayer ferromagnetism to intralayer antiferromagnetism in $Sr_4Ru_3O_{10}$. *Phys. Rev. B* **98**, 064418 (2018).
22. Zhao, H. D. et al. Nonequilibrium orbital transitions via applied electrical current in calcium ruthenates. *Phys. Rev. B* **100**, 241104(R) (2019).
23. Cao, Y. et al. Hallmarks of the Mott-metal crossover in the hole doped $J = 1/2$ Mott insulator Sr_2IrO_4. *Nat. Commun.* **7**, 11367 (2016).
24. Lindquist, A. W. & Kee, H. Y. Odd-parity superconductivity driven by octahedra rotations in iridium oxides. *Phys. Rev. B* **100**, 054512 (2019).
25. Ye, F. et al. Pseudospin-lattice coupling and electric control of the square-lattice iridate Sr_2IrO_4. *Phys. Rev. B* **102**, 115120 (2020).
26. Steiner, U. E. & Ulrich, T. Magnetic field effects in chemical kinetics and related phenomena. *Chem. Rev.* **89**, 51–147 (1989).
27. Dold, P., Croll, A. & Benz, K. W. Floating-zone growth of silicon in magnetic fields, I. Weak static axial fields. *J. Cryst. Growth* **183**, 545–553 (1998).
28. Dold, P. & Benz, K. W. Modification of fluid flow and heat transport in vertical Bridgman configurations by rotating magnetic fields. *Cryst. Res. Technol.* **32**, 51–60 (1997).
29. Series, R. W. & Hurle, D. T. J. The use of magnetic fields in semiconductor crystal growth. *J. Cryst. Growth* **113**, 1–2 (1991).
30. Wakayama, N. I. Effects of a strong magnetic field on protein crystal growth. *Cryst. Growth Des. 2003* **3**(1), 17–24 (2002).
31. Wilkens, J. & Müller-Buschbaum, H. K. Zur Kenntnis von $Ba4Ir_3O_{10}$. *Z. F.ür. Anorg. Allg. Chem.* **592**, 79–83 (1991).
32. Cao, G., Bolivar, J., McCall, S., Crow, J. E. & Guertin, R. P. Weak ferromagnetism, metal-to-nonmetal transition and negative differential resistivity in single crystal Sr_2IrO_4. *Phys. Rev. B* **57**, R11039–R11042 (1998).
33. Cao, G., McCall, S., Shepard, M., Crow, J. E. & Guertin, R. P. Magnetic and transport properties of single crystal Ca_2RuO_4: Relationship to superconducting Sr_2RuO_4. *Phys. Rev. B* **56**, R2916–R2919 (1997).
34. Cao, G. et al. Quantum liquid from strange frustration in the trimer magnet $Ba_4Ir_3O_{10}$. *npj Quantum Mater.* **5**, 26 (2020).
35. Alexander, C. S. et al. Destruction of the Mott insulating ground state of Ca_2RuO_4 by a structural transition. *Phys. Rev. B* **60**, R8422–R8425 (1999).
36. Braden, M., André, G., Nakatsuji, S. & Maeno, Y. Crystal and magnetic structure of Ca_2RuO_4: Magnetoelastic coupling and the metal-insulator transition. *Phys. Rev. B* **58**, 847 (1998).
37. Steffens, P. et al. High-pressure diffraction studies on Ca_2RuO_4. *Phys. Rev. B* **72**, 094104 (2005).
38. Fang, Z. & Terakura, K. Magnetic phase diagram of $Ca_{2-x}Sr_xRuO_4$ governed by structural distortions. *Phys. Rev. B* **64**, 020509 (R) (2001).
39. Lee, J. S. et al. Electron and Orbital Correlations in $Ca_{2-x}Sr_xRuO_4$ Probed by Optical Spectroscopy. *Phys. Rev. Lett.* **89**, 257402 (2002).
40. Jung, J. H. et al. Change of electronic structure in Ca_2RuO_4 induced by orbital ordering. *Phys. Rev. Lett.* **91**, 056403 (2003).
41. Gorelov, E. et al. Nature of the Mott transition in Ca_2RuO_4. *Phys. Rev. Lett.* **104**, 226401 (2010).
42. Liu, G. Q. Spin-orbit coupling induced Mott transition in $Ca_{2-x}Sr_xRuO_4$ ($0 \le x \le 0.2$). *Phys. Rev. B* **84**, 235136 (2011).
43. Cao, G. et al. Ground-state instability of Mott insulator Ca_2RuO_4: impact of slight La-doping on metal-insulator transition and magnetic ordering. *Phys. Rev. B* **61**, R5053–R5057 (2000).
44. Zegkinoglou, I. et al. Orbital ordering transition in Ca_2RuO_4 observed with resonant X-ray diffraction. *Phys., Rev. Lett.* **95**, 136401 (2005).
45. Snow, C. S. et al. Pressure-tuned collapse of the Mott-like state in $Ca_{n+1}Ru_nO3_{n+1}$ ($n = 1,2$): Raman spectroscopic studies. *Phys. Rev. Lett.* **89**, 226401 (2002).
46. Qi, T. F. et al. Negative volume thermal expansion via orbital and magnetic orders in single-crystal $Ca_2Ru_{1-x}Cr_xO_4$. *Phys. Rev. Lett.* **105**, 177203 (2010).
47. Kim, B. J. et al. Novel $J_{eff} = 1/2$ Mott state induced by relativistic spin-orbit coupling in Sr_2IrO_4. *Phys. Rev. Lett.* **101**, 076402 (2008).
48. Kim, B. J. et al. Phase-sensitive observation a spin-orbital Mott state *Sr_2IrO_4*. *Science* **323**, 1329–1332 (2009).
49. Chen, C. et al. Persistent insulating state at megabar pressures in strongly spin-orbit-coupled Sr_2IrO_4. *Phys. Rev. B* **101**, 144102 (2020).
50. Yang, J. A. et al. High-energy electronic excitations in Sr_2IrO_4 observed by Raman scattering. *Phys. Rev. B* **91**, 195140 (2015).
51. Nussinov, Z. & van den Brink, J. Compass models: theory and physical motivations. *Rev. Mod. Phys.* **87**, 1–59 (2015).

ACKNOWLEDGEMENTS

This work is supported by NSF via grants DMR 1903888. Raman scattering work (N.P. and D.R.) was supported by the NSF under Grant No. DMR-1709946. G.C. is thankful to Drs. Dan Dessau, Minhyea Lee, Feng Ye, and Lance DeLong for useful discussions.

AUTHOR CONTRIBUTIONS

G.C. initiated and directed the project; he also grew the single crystals, performed measurements of physical properties and data analysis, and wrote the paper with input from all authors. H.D.Z and B.H. performed measurements of heat capacity, resistivity and magnetization and data analysis. H.D.Z also performed measurements of the crystal structure using single-crystal X-ray diffraction and data analysis. N.P. performed measurements of Raman scattering and data analysis and D.R. directed these measurements and provided the analysis of the Raman scattering data and other data. P.S. provided critical insights into the physics of the field-editing technology. I.K. developed the theoretical scenario for the phenomena.

COMPETING INTERESTS

The authors declare no competing interests.

ADDITIONAL INFORMATION

Supplementary information is available for this paper at https://doi.org/10.1038/s41535-020-00286-2.

Correspondence and requests for materials should be addressed to G.C.

Reprints and permission information is available at http://www.nature.com/reprints